

# Refraction contrast 11×-magnified X-ray imaging of large objects by MIRRORCLE-type table-top synchrotron

Toru Hirai,<sup>a</sup> Hironari Yamada,<sup>a,b,c\*</sup> Makoto Sasaki,<sup>a</sup> Daisuke Hasegawa,<sup>c</sup> Masaki Morita,<sup>c</sup> Yasuhito Oda,<sup>a</sup> Jyunya Takaku,<sup>a</sup> Takayasu Hanashima,<sup>b</sup> Norihisa Nitta,<sup>d</sup> Masashi Takahashi<sup>d</sup> and Kiyoshi Murata<sup>d</sup>

<sup>a</sup>Faculty of Science and Engineering, Ritsumeikan University, 1-1-1 Nojihigashi, Kusatsu, Shiga 525-8577, Japan, <sup>b</sup>Synchrotron Light Life Science Centre, Ritsumeikan University, 1-1-1 Nojihigashi, Kusatsu, Shiga 525-8577, Japan, <sup>c</sup>Photon Production Laboratory Ltd, 4-2-1(808) Takagaicho Minami, Omihachiman, Shiga 523-0898, Japan, and <sup>d</sup>Department of Radiography, Shiga University of Medical Science, Ohtsu, Shiga 520-2192, Japan.  
E-mail: hironari@se.ritsumei.ac.jp

The high-quality aspects of magnified X-ray images recorded using MIRRORCLE-6X are reported. MIRRORCLE-6X is inherently suitable for hard X-ray imaging owing to its magnified projection X-ray imaging, micrometre-size X-ray source point, wide radiation emission angle, X-ray spectrum ranging from 10 keV to 6 MeV, natural refraction contrast imaging and high flux output. Images produced with 11× geometrical magnification display a sharply enhanced edge effect when generated using a 25 µm rod electron target. Image contrast is enhanced 2× owing to refraction when compared with absorption contrast images. An imitation tumour implanted in a human chest phantom was made clearly visible by using edge enhancement on images. Soft tissue becomes highly visible as a natural consequence of refraction contrast when using hard X-rays for imaging. The authors believe that novel imaging provided by MIRRORCLE makes it a superior instrument for medical diagnosis.

## 1. Introduction

A synchrotron radiation source is known for its fine spatial resolution and phase-contrast imaging by its highly monochromatic parallel beam (Suzuki *et al.*, 1999, 2002; Kagosima *et al.*, 1999; Yagi *et al.*, 1999). A micro-focus point (MFP) source is known for its large magnification owing to the micrometre-size emission point (Wilkins *et al.*, 1996). Application of a synchrotron radiation source is, however, limited to small specimens, up to 80 mm × 150 mm exposure field (Hyodo *et al.*, 1998) at a distance of 45 m from the source point. Application of the MFP source is limited to small specimens at short distances because of the low exposure rate as a result of limited X-ray power. In the case of the MIRRORCLE-type synchrotron (Yamada, 2003, 1998, 1996), however, we are able to record human-size images. Its high power enables a short exposure time. With MIRRORCLE, the target in the synchrotron orbit determines the effective source size. Consequently it can be of a micrometre-order size since it does not suffer from most of the limiting factors of conventional

X-ray source targets. High brilliance can be obtained because the relativistic electrons are recirculating and refreshed by an accelerating cavity. The stored beam current reaches several amperes. The radiation angle is determined by the kinematics  $1/\gamma$  owing to the same principle governing conventional synchrotron radiation. MIRRORCLE-6X is, however, based on a low-energy synchrotron, and thus provides a large area of irradiation. The obtained irradiation area has a diameter of 340 mm at a distance of 2 m from the source point. White hard X-rays are generated. The X-ray energy spectrum reaches that of the circulating electron energy (6 MeV), and is higher than that at synchrotron radiation X-ray sources. We can tune the X-ray spectral distribution in the low-energy region by changing the material and the thickness of the target. Fig. 1 shows typical shapes of the X-ray target. We know the Bremsstrahlung spectrum from the Monte Carlo simulation code *GEANT4* (Agostinelli *et al.*, 2003) as shown in Fig. 2 for the case of a 6 MeV electron beam and different materials and thicknesses. The average X-ray energy is high when the atomic number and the thickness of the X-ray target are large. X-ray

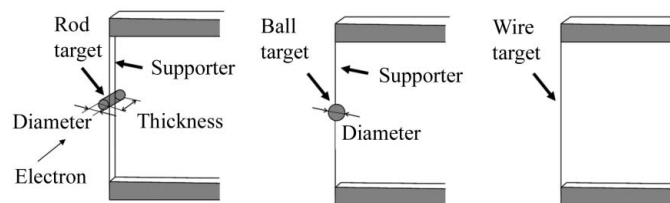


**Figure 1**  
Typical shapes of the X-ray target. The effective emitter point is defined by the cross section of the rod target or ball facing the electron beam.

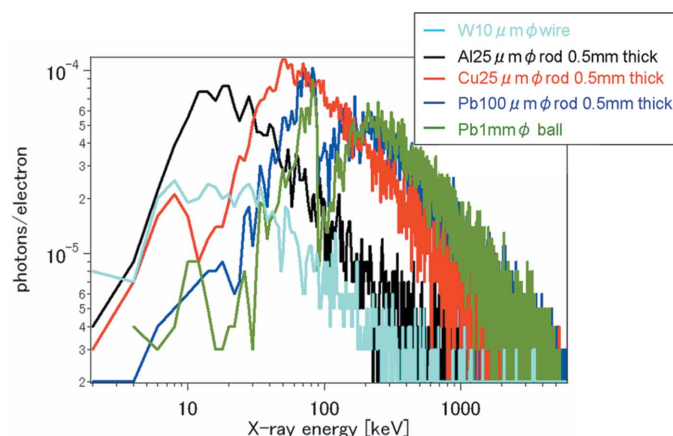


**Figure 2**  
X-ray spectrum calculated using the Monte Carlo simulation code *GEANT4* for 6 MeV electrons.

beam features generated by MIRRORCLE-6X are useful for magnified X-ray imaging of large objects. We can achieve high spatial resolution and large magnification simultaneously by decreasing the target size (Yamada *et al.*, 2006); 2.5 μm is so far the smallest we have achieved with a relatively high X-ray flux. Furthermore, a small source point is expected to show edge enhancements owing to refraction contrast. It is reported that a small source point size and large distance between object and detector appear to be essential for phase-contrast imaging (Yada & Takahashi, 1990; Kagosima *et al.*, 1999; Ishisaka *et al.*, 2000). In this paper we evaluate the refraction contrast image recorded using MIRRORCLE-6X with a 10 μm-diameter wire target. Edge enhancement appears in images recorded using the white X-ray beam of MIRRORCLE-6X; it is especially observed in higher magnification images. In this paper we demonstrate the edge-enhanced highly magnified images.

## 2. Experimental set-up and results

### 2.1. Magnified imaging

Fig. 3 indicates a simple experimental set-up for magnified X-ray imaging. A source point, specimen and imaging device are aligned. The distances between the X-ray source point and the sample ( $L_1$ ) and the sample and the imaging device ( $L_2$ ) are adjustable from 0.25 m to 5 m (room size limit). We can easily change the magnification by changing the ratio  $L_1/L_2$

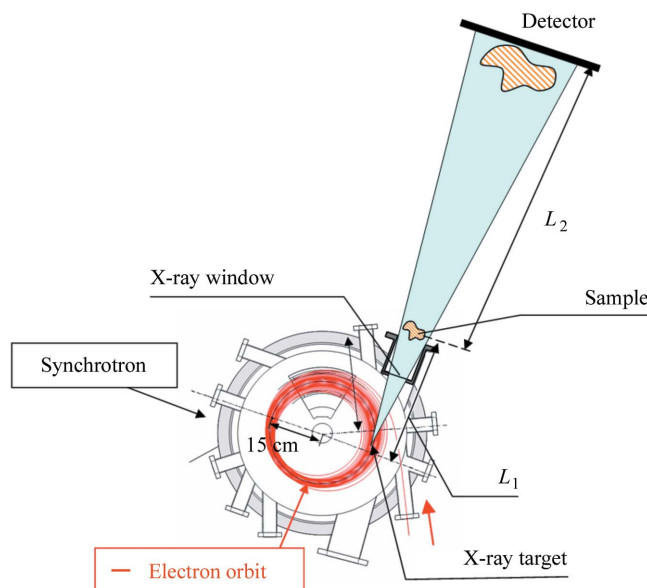


**Figure 3**  
Experimental arrangement for the magnified X-ray imaging. The magnification rate is determined by  $L_1$ , the distance between the X-ray source and the sample, and  $L_2$ , the distance between the specimen and the detector.

from 1 to 12. We use an imaging plate (IP) with pixel size 150 μm (Fuji Film, model FCR-XG1).

We have performed magnified X-ray imaging of a 25 cm-thick human chest phantom as shown in Fig. 4. This phantom includes a human lung, ribs and a number of knots imitating a tumour made of urethane of diameter 8 mm. The target was a 25 μm-diameter 0.5 mm-thick Cu rod placed pointing in the beam direction. Fig. 4(a) represents the contacted image, Fig. 4(b) the 5×-magnified image and Fig. 4(c) the 11×-magnified image. The X-ray source–specimen distance  $L_1$  was set at 0.45 m for the 11× magnification. The knots, ribs and a number of vessels are clearly seen. The characteristics of a refraction contrast image are clearly shown at the bone and tumour edges. Vessels are soft tissues but are visible because of the phase contrast. In the case of a conventional X-ray tube for medical use, it has been shown that it is impossible to distinguish the tumour in the precise shape. An 11× magnification is impossible using a conventional X-ray tube because of increased penumbral blur caused by the millimetre-order target. A millimetre-size tumour should be clearly visible since the 8 mm knots in Figs. 4(b) and 4(c) are identifiable by their shape. Experience of magnified imaging has been gained in X-ray microscopy of cytoplasm (Hoshino & Aoki, 2006; Hirai *et al.*, 1999; Yada & Takahashi, 1990). Magnified imaging has only been previously available for small and thin objects, but the magnified imaging of large objects, *e.g.* humans, has become practical with MIRRORCLE-6X. Magnified phase contrast is the key to this fine imaging.

### 2.2. Degree of the edge enhancement

Phase-contrast imaging is now widely used at synchrotron radiation sources. It is generally thought that a highly parallel and monochromatic X-ray beam is desirable. Edge enhance-

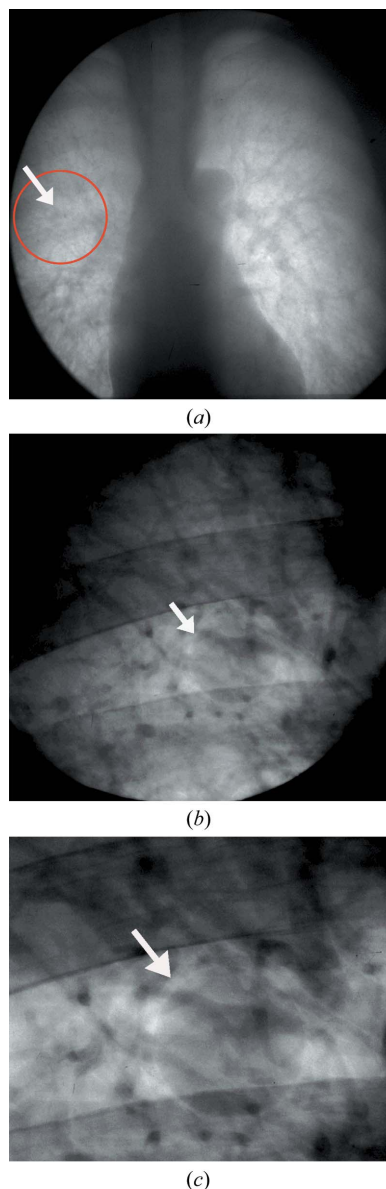


**Figure 4**  
Medical diagnosis of a chest phantom recorded using MIRRORCLE-6X. (a) Contacted X-ray image, (b) 5 $\times$ -magnified X-ray image, (c) 11 $\times$ -magnified image. The imitation tumour behind the bone made of urethane (indicated by the arrow) is visible by its enhanced edge resulting from the refraction contrast. Bone is also recognized by its edge. The black spots are cross sections of vessels.

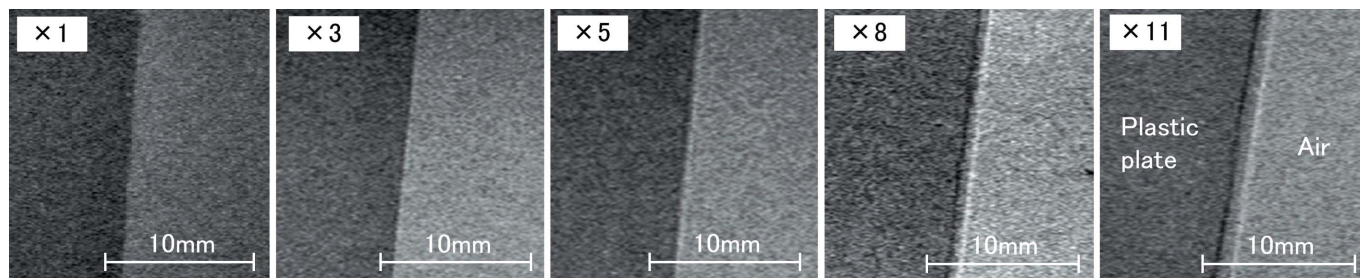


**Figure 5**  
X-ray images of a 2 mm-thick plastic plate at the edge recorded using MIRRORCLE. Dark and bright lines are the enhanced edge due to the refraction contrast. The magnification is shown at the top left-hand corner of each image.

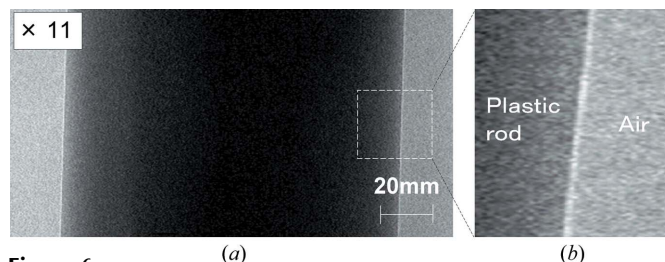


**Figure 6**  
(a) Refraction magnified X-ray image of a 10 mm-diameter rod recorded using MIRRORCLE for 11 $\times$  magnification. (b) Detail of the fringe pattern. Since the object is rod-shaped, only a bright line appears.

ment also appears with polychromatic micro-focus X-ray sources. Polychromatic hard X-rays are generated by MIRRORCLE-6X. We found that the edge effect is more enhanced with higher magnification. In the following we study the nature of the edge enhancement by MIRRORCLE. We have taken the image of a 2 mm-thick plastic plate as well as a 1 cm acrylic rod. The samples are placed at  $L_1 = 0.44$  m from the source point with the IP at distance  $L_2$ . The X-ray total exposure dose at the IP is controlled so as to be equal for every image taken at different distances. As shown in Fig. 5, we clearly see a pair of bright and dark lines along the boundaries between the plastic plate and air in all images except the contact image (noted as  $\times 1$ ). We see that the distance between the bright and dark lines increases proportionally as the magnification increases. In Fig. 6 an 11 $\times$ -magnified image of a plastic rod is shown. In this case we only see a bright line along the edge of the plastic rod because absorption increases at the centre of the rod. Fig. 7 shows profiles of the plastic plate along a line perpendicular to the edge. The peak height, both positive and negative, is most enhanced with the largest magnification, *i.e.* 11 $\times$ . It is clear that the enhancement is larger as the magnification is larger or the distance between the sample and the detector is longer. It is noted that the irradiation dose rate is set to a constant for the different magnifications at the position where the direct X-rays are observed. Thus the absorption rate is almost the same for each profile. We see here that the absorption rate is constant but the peak height increases as the magnification increases.

These edges are characterized by three parameters: peak height,  $\Delta I$ , peak position,  $\Delta X$ , and width,  $\Delta W$ , as shown in Fig. 7. The width  $\Delta W$  is defined as the distance between the

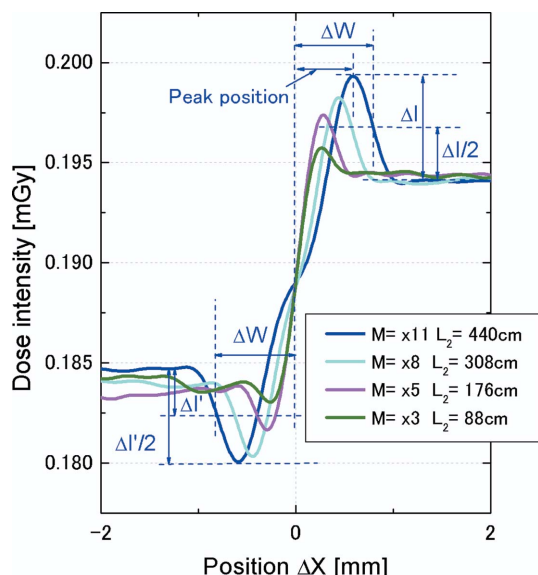


**Figure 7**  
Intensity profile of the enhanced edges. The sample is a 2 mm-thick plastic plate. The width and the peak position increase with the magnification. Notation  $\Delta I$  for the peak height and  $\Delta W$  for the width are defined.

centre and the point of the half maximum (see Fig. 7). The peak position is defined as the distance from the centre. Summarized peak positions and widths, together with geometrical penumbral blurs, and peak height are shown as a function of the sample–detector distance  $L_2$  in Figs. 8 and 9, respectively. The peak position and the width increase almost linearly as the distance increases, except for the data at  $L_2 = 88$  cm; we think that the contribution from the low-energy X-ray flux is significant at the short distance. Ignoring this contribution, the peak position and the width cross the zero point when  $L_2$  is zero. The low-energy X-rays show larger deflection. This is the reason for the larger values of the width and peak position at short  $L_2$  distances.

It is known that an edge-enhanced image can be observed by setting the detector at an appropriate distance from the object and can be observed while the peak width  $\Delta W$  is larger than the penumbral blurring. We demonstrate in Fig. 8 that the width  $\Delta W$  is significantly larger than the penumbral blurring and is proportional to the distance. In our case the blurring is defined by the target size. In the case of MIRRORCLE, the edge enhancement appears at an object-to-detector distance of more than 0.88 m ( $\times 3$ ), and is more enhanced at the longer distances. The detector resolution never limits the refraction contrast in the MIRRORCLE imaging because of the magnification. Also note that the deflection angle becomes larger when it has a larger incidence angle to the boundary interface. The peak height increases as the distance  $L_2$  increases.

The quality of an image in terms of contrast may be evaluated as follows: the refraction contrast is defined as  $A_{\max}/A_{\min}$  and the absorption contrast is defined as  $B_{\max}/B_{\min}$ , which are indicated in Fig. 10(a). As we see from Fig. 10(b), in the case of 11 $\times$ -magnified imaging with MIRRORCLE, the quality of the refraction contrast image increases as the

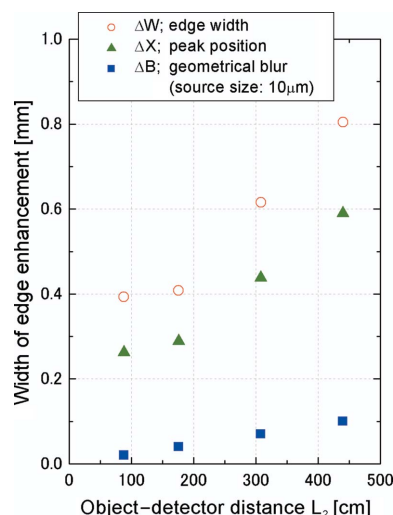


**Figure 8**  
The widths  $\Delta W$  and the peak positions  $\Delta X$  of the enhanced edges are plotted as a function of the distance  $L_2$ ; both increase linearly with  $L_2$ . The increase of the geometrical penumbral blurring due to the source size is also indicated.  $\Delta B$  is determined by the source size ( $d$ ), the distance between the source and object ( $L_1$ ) and the distance between the object and the image plane ( $L_2$ ). It is calculated as  $\Delta B = dL_2/L_1$ .

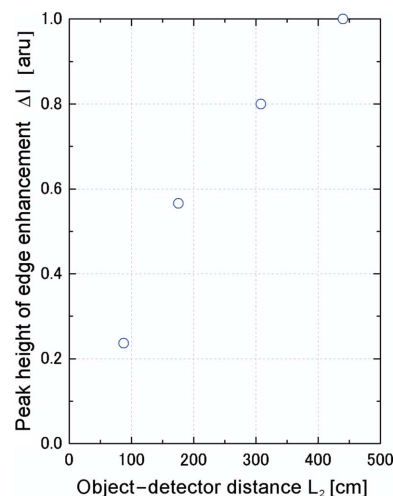


**Figure 9**  
Peak heights  $\Delta I$  of the enhanced edges are plotted as a function of distance  $L_2$ ;  $\Delta I$  increases quadratically with  $L_2$ .

magnification increases to nearly twice the absorption contrast. It is apparent that the refraction contrast is much higher than the absorption contrast.

### 2.3. Edge enhancement by the geometrical refraction of X-rays

We have carefully analyzed the deflection angle of the enhanced edges. Evaluation of the edge enhancement can be studied using geometrical optics because the effect of diffraction is negligibly small compared with the spatial resolution,  $\Delta r \geq (\lambda L_2)^{1/2}$ , where  $\lambda$  is the X-ray wavelength and  $\Delta r$  is the total spatial resolution of this imaging system. The limit of geometrical optics is given by Fresnel’s formula of diffraction (Born & Wolf, 1975). The direction of the X-rays is

slightly deflected at the interfaces in accordance with Snell's law of refraction. The geometrical optics are shown in Fig. 11. The obtained deflection angle, which corresponds to angle  $\theta$  in Fig. 11, is calculated for several different positions  $\Delta X$  within the edge, such as the peak and the maximum points.  $\theta$  is given as

$$\theta = \tan^{-1}[(X + \Delta X - \chi)/(L_2 - t)] - \tan^{-1}[\chi/(L_1 + t)],$$

where  $X$  is the distance of the observed edge from the centre of the image,  $\chi$  is the object edge (12 mm) measured from its centre, and  $t$  is the thickness (1 mm) of the object (see Fig. 11). We obtain, for the 2 mm-thick plastic plate,  $2.5 \times 10^{-4}$  rad at the maximum and  $1.5 \times 10^{-4}$  rad at the peak. The minimum is difficult to define. The corresponding X-ray energy giving this deflection angle is 10 keV for the maximum deflection and 15 keV for the peak position. We take into account that the largest X-ray incident angle to the edge is  $1.56^\circ$  and the refractive index,  $\delta$ , is  $4.6 \times 10^{-6}$  and  $5.0 \times 10^{-7}$  for 10 keV and 30 keV, respectively. The width of the edge is rather large compared with the results from the synchrotron radiation

experiment because the X-ray energy is largely spread from 10 to nearly 50 keV in the case of MIRRORCLE. So the lowest, *i.e.* 10 keV, X-ray flux is contributing to the enhanced edge. The highest energy should go up to 50 keV according to the simulation for the W target shown in Fig. 2.

The magnitude of the refraction contrast, as demonstrated in Fig. 10, increases as the magnification increases. We have observed an increased refraction contrast with large sample-detector distances. Suzuki *et al.* (1999) and Ishisaka *et al.* (2000) have suggested that the refraction contrast will be enhanced while the detector resolution is increased. We have observed this enhancement with a small target size and magnified imaging. The maximum contrast that can be obtained with conventional imaging is given by the spatial resolution,  $\Delta r = (\lambda L_2)^{1/2}$  (Suzuki *et al.*, 1999). In MIRRORCLE imaging the spatial resolution  $\Delta r$  also encountered this limit during magnified imaging.

The magnified X-ray imaging capabilities of MIRRORCLE are a great advantage to medical imaging as shown by the chest phantom image in Fig. 4.

### 3. Conclusion

We have shown that MIRRORCLE is a new brilliant X-ray source that is different from either a synchrotron radiation source or an X-ray tube. MIRRORCLE provides a diverging beam from a micrometre-order point source similar to a micro-focus X-ray source, not a parallel beam like with a synchrotron radiation source. Features of the X-rays generated by MIRRORCLE-6X are useful for magnified X-ray imaging of large objects. We achieve higher resolution and higher edge enhancement with larger magnification by using a small source point. The small source point is a powerful aid for refraction contrast imaging; it appears to be essential for refraction contrast imaging instead of a parallel beam.

It is demonstrated that MIRRORCLE-6X provides a tremendous improvement in medical imaging capability. A millimetre-size tumour can be clearly seen in the magnified images, without any aids to enhance the absorption rate, because of refractive contrast. Large-object magnified imaging is also more appropriate for existing 150  $\mu\text{m}$ -size pixel digital devices such as imaging plates or flat panels. Our next goal will be 100 $\times$  to 1000 $\times$  magnification with a submicrometre target.

### References

- Agostinelli, S., Allison, J. & Amako, K. (2003). *Nucl. Instrum. Methods Phys. Res. A*, **506**, 250–303.
- Born, M. & Wolf, E. (1975). *Principles of Optics*, 5th ed. Oxford: Pergamon Press.
- Hirai, A., Takemoto, K., Nishino, K., Niemann, B., Hettwer, M., Rodolph, D., Anderson, E., Attwood, D., Kern, D., Nakayama, Y. & Kihara, H. (1999). *Jpn. J. Appl. Phys.* **138**, 274–278.

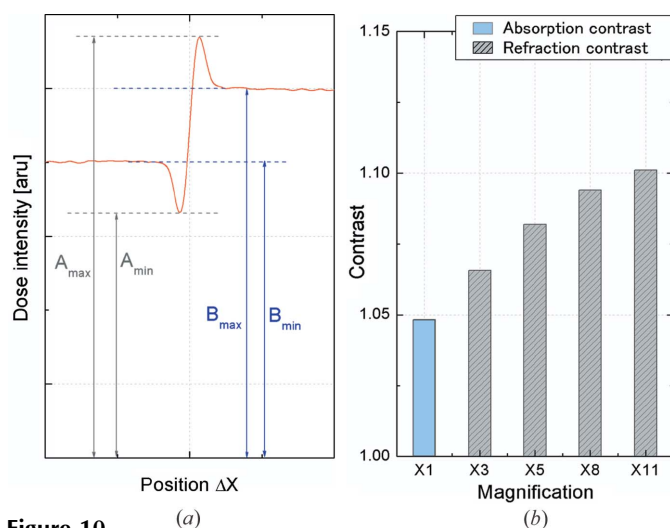


**Figure 10** (a) Intensity profile of typical refraction contrast imaging. Notations  $A_{\max}$ ,  $B_{\max}$ ,  $A_{\min}$  and  $B_{\min}$  for dose intensity at the image plane are defined. (b) The 11 $\times$  refraction contrast of magnified imaging is twice as large as that of the absorption contrast.

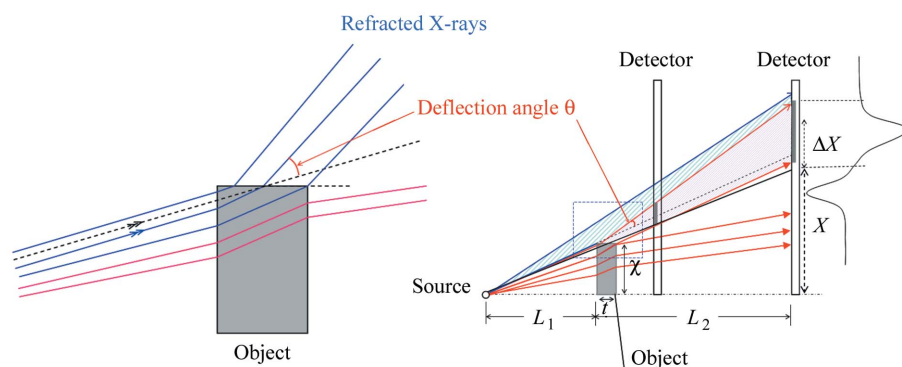


**Figure 11** Schematic view showing the refraction of the X-rays and the deflection angle.

- Hoshino, M. & Aoki, S. (2006). *Jpn. J. Appl. Phys.* **45**, 989–994.
- Hyodo, K., Ando, M., Oku, Y., Yamamoto, S., Takeda, T., Itai, Y., Ohtsuka, S., Sugishita, Y. & Tada, J. (1998). *J. Synchrotron Rad.* **5**, 1123–1126.
- Ishisaka, A., Ohara, H. & Honda, C. (2000). *Opt. Rev.* **7**, 566.
- Kagosima, Y., Tsusaka, Y., Yokoyama, K., Takai, K., Takeda, S. & Matsui, J. (1999). *Jpn. J. Appl. Phys.* **38**, L470–L472.
- Suzuki, Y., Yagi, N. & Uesugi, K. (2002). *J. Synchrotron Rad.* **9**, 160–165.
- Suzuki, Y., Yagi, N., Umetani, K., Kohmura, Y. & Yamasaki, K. (1999). *Proc. SPIE*, **3770**, 13–22.
- Wilkins, S., Gureyev, T., Gao, D., Pogany, A. & Stevenson, A. (1996). *Nature (London)*, **384**, 335–338.
- Yada, K. & Takahashi, S. (1990). *X-ray Microscopy in Biology and Medicine*, p. 193. Tokyo: Japan Scientific Societies Press/Berlin: Springer Verlag.
- Yagi, N., Suzuki, Y., Umetani, K., Kohmura, Y. & Yamasaki, K. (1999). *Med. Phys.* **26**, 2190–2193.
- Yamada, H. (1996). *Jpn. J. Appl. Phys.* **35**, L182–L185.
- Yamada, H. (1998). *J. Synchrotron Rad.* **5**, 1326–1331.
- Yamada, H. (2003). *Nucl. Instrum. Methods Phys. Res. B*, **199**, 509–516.
- Yamada, H., Hirai, T., Sasaki, M., Hasegawa, D., Oda, Y. & Takaku, J. (2006). *Proceedings of the 8th International Conference on X-ray Microscopy*, 26–30 July 2005, Himeji, Japan, pp. 130–132. Tokyo: Institute of Pure and Applied Physics.